Geocarto International

ISSN: (Print) (Online) Journal homepage: https://www.tandfonline.com/loi/tgei20

Spatially varying WIndow based maximum likelihood Feature Tracking (SWIFT) Method for Glacier Surface Velocity Estimations

S. Tomar Sangita, Raaj. Ramsankaran & Jeffrey P. Walker

To cite this article: S. Tomar Sangita, Raaj. Ramsankaran & Jeffrey P. Walker (2022): Spatially varying WIndow based maximum likelihood Feature Tracking (SWIFT) Method for Glacier Surface Velocity Estimations, Geocarto International, DOI: 10.1080/10106049.2022.2082556

To link to this article: https://doi.org/10.1080/10106049.2022.2082556

Spatially varying WIndow based maximum likelihood Feature Tracking (SWIFT) Method for Glacier Surface Velocity Estimations

Sangita S. Tomar[a, b, c], RAAJ. Ramsankaran*[b], Jeffrey P. Walker [c]

[a]IITB-Monash Research Academy, Mumbai 400076, Maharashtra, India

[b]Hydro-Remote Sensing Applications (H-RSA) Group, Department of Civil Engineering, Indian Institute of Technology Bombay, Mumbai 400076, Maharashtra, India

[c]Department of Civil Engineering, Monash University, Melbourne, VIC 3800, Australia

*Corresponding authors;

Email: ramsankaran@civil.iitb.ac.in, singh.sangita15@gmail.com

Spatially varying WIndow based maximum likelihood Feature Tracking (SWIFT) Method for Glacier Surface Velocity Estimations

Glacier surface velocity is an important variable for glacier dynamics studies. Estimation of accurate surface velocity from remote sensing is a challenge, especially for glaciers with no in-situ observations. To overcome this challenge, a new method for glacier feature tracking named as SWIFT (Spatially varying WIndow based maximum likelihood Feature Tracking) has been proposed. This method utilises both optical data (to automatically determine the window size using the concept of Object Based Image Analysis) and Synthetic Aperture Radar (SAR) data (to perform feature tracking). The proposed method uses a spatially varying window size unlike other existing softwares that cannot provide the flexibility of a spatially varying window size. The proposed method has been tested and validated at three different glaciers (South Glacier, Canada; Chhota Shigri Glacier, India; and Tasman Glacier, New Zealand) for which field measured data were available. The obtained results for all three glaciers showed consistent improvement in estimated velocity by SWIFT when compared with spatially fixed window size-based estimates from normalized cross correlation-based Correlation Image Analysis Software (CIAS). Considering the data availability, the proposed SWIFT method has been implemented using a variety of SAR and optical satellite data to understand its performance/effectiveness for glacier surface velocity estimation. When validated against field measurements, the results from SWIFT gave an RMSE of 12.8 m/yr, 15.32 m/yr and 67.1 m/yr for South Glacier, Chhota Shigri Glacier and Tasman Glacier, respectively. Moreover, the RMSE of SWIFT estimates were observed to have an RMSE that was 19%-36% lower than the best performing spatially fixed window size.

Keywords: Glacier surface velocity; Feature tracking approach; SAR; Optical; Automated window size

1. Introduction

Glacier velocity is one of the paramount variables that impact glacier dynamics. Glacier velocity comprises three components: surface velocity, sub-surface velocity and basal sliding. Among these components, the glacier surface velocity can be monitored using remote sensing to overcome the challenge of inaccessibility and weather dependent data collection encountered in collecting field measurements. Moreover, glacier surface velocity at annual or decadal scale represents the overall stress regime of a glacier, which in turn is an indicator of its geometric characteristics like ice-thickness (McNabb et al., 2012). The surface velocity can also distinguish active from inactive ice on debris-covered glaciers, identify glacier surge events, and even infer basal conditions. However, there remain challenges to routine monitoring of glacier surface velocity globally.

Existing approaches for glacier surface velocity monitoring include ground surveys, Interferometric Synthetic Aperture Radar (InSAR) techniques, and image matching techniques using either optical or Synthetic Aperture Radar (SAR) imagery. The ground-based survey is the most accurate method but confines the measurements to limited parts of a glacier due to logistical reasons and can only be conducted during a specific time of year and when there are favourable weather conditions. Studies have shown the potential of the InSAR technique for glacier velocity estimation (Palmer et al., 2010; Kumar et al., 2011; Sánchez-Gámez and Navarro 2017; Tong et al., 2018). Though the precision of velocity estimation through InSAR can reach to millimetres, its successful application is often limited by phase noise and large displacements over time (Pritchard et al., 2005; Joughin et al., 2010). Other techniques for glacier velocity estimation comprise of image matching based glacier feature tracking where the shift in a glacier is derived from the best match between corresponding pairs of images. Both SAR and optical imagery can be utilized by this technique. Using SAR, the glacier velocity can be estimated by tracking the amplitude (Derauw, 1999; Strozzi et al., 2002; Ciappa et al., 2010; Riveros et al., 2013), intensity (Ruan et al., 2013; Sanchez-Gamez and Navarro 2017; Yellala et al., 2019), speckle (Short and Gray 2005) or coherence (Strozzi et al., 2002) of the images. The SAR image pairs used in these studies are either

separated by a few days or a few months. Yellala et al. (2019) successfully demonstrated an application of SAR-based feature tracking using a SAR data pair at one year apart. Likewise, optical images have also been used for glacier feature tracking using the digital numbers that represent visual features on a glacier surface (Kaab et al., 2002; Scherler et al., 2008; Heid and Kaab, 2012; Messerli and Grinsted, 2015, Fahnestock et al., 2016), but they often suffer due to presence of cloud cover over the glaciated regions.

The studies using either SAR or optical data consider the correlation between two temporal images as a similarity measure to estimate the shift between images. Recently, there were some improvements in cross correlation-based glacier feature tracking using techniques like Particle Image Velocimetry (Patel et al., 2019) and thin plate smooth splines (Ruan et al., 2013) to eliminate erroneous velocity values. Apart from the correlation, other similarity measures such as maximum likelihood have been used to study glacier flow using remote sensing data, with Erten et al. (2009) and Deledalle et al. (2011) performing comparative studies to assess the accuracy of maximum likelihood-based tracking with classical correlation-based tracking, and found the former to be the more robust approach.

Existing approaches for glacier feature-tracking using repeat satellite imagery allow displacements to be found with better precision than a single pair imagery. Although improved, these methods consume more resources (time and storage space) and are still prone to human error by requiring manual inputs (Ahn and Howat, 2011). A basic concern for any image matching based feature tracking method, including the aforementioned image matching based approaches is to determine an optimum window size for image matching. Studies by Huang and Li (2011) and Turrin et al. (2013) have shown that use of a different feature tracking window size leads to different velocity estimates for the same glacier. With an uncertain image matching window size, the velocity estimates have to be presented either at different window sizes (Huang and Li, 2011; Schubert et al., 2013; Chen et al., 2017) or at a window size which is calibrated using known glacier velocity information (Riveros et al., 2013). At present, calibration of window size is a challenge where no glacier velocity measurements are available. This introduces a significant level of uncertainty in remote sensing-based glacier

velocity estimation (Kumari et al., 2019). In this respect, a spatially variable window size can help reduce the errors in glacier velocity estimation. Recently, large scale study on glacier velocity estimation demonstrated application of a spatially variable window size using auto Repeat Image Feature Tracking (auto-RIFT) (Dehecq et al., 2019), where they used three different search window sizes over a scene -- namely: 240 m×240 m (image pixels located within a 2 km buffer of a glacier); 480 m×480 m (image pixels located more than 2 km from a glacier) and 960 m×960 m (for unsuccessful searches). However, here a variable window size was not explored within the glacier region. Similarly, other methods which are available within freely distributed software such as CIAS (Kaab and Vollmer, 2000), GIV (Van Wyk de Vries and Wickert 2021) and ImCorr (Scambos et al., 1992) have not used spatially variable windows. For a more glacier specific and realistic estimation, Dehecq et al., (2019) and Kumari et al., (2019) stated that the window size needs to be spatially variable (within a glacier) depending upon the glacier features or glacier size, but was not explored in their earlier studies.

To address this issue of automatically determining a spatially varying window size for image matching, a simple innovative method based on the concept of Object Based Image Analysis (OBIA) is proposed. Here, the proposed method utilises various attributes of optical image features (or image segments). A wide range of researchers have used OBIA to segment and classify images, demonstrating the immense potential of this class of image analysis in remote sensing (Blaschke et al., 2010; Chen et al., 2018). As compared to the pixel-based operations where the spatial attributes are not considered, the OBIA increases the image interpretation by considering different aspects of an image segment. It is important to note that this concept has not been exploited to date for glacier feature tracking studies. Therefore, this novel approach of window size determination is integrated with the remote sensing-based feature tracking method to estimate glacier surface velocity, with the proposed method conceptualized to extract useful information from both optical and SAR sensors. The first stage of the method is about automated window size determination from OBIA of an optical image, while the second stage is the implementation of a SAR based glacier feature tracking method using the maximum likelihood (ML) of SAR speckle as a similarity measure. This proposed method has been tested over three different glaciers from different

regions of the world, and its performance assessed in view of different satellite sensors and time of acquisition of imagery over certain topographical zones and glacier facies. Finally, a comparative analysis was done against the spatially fixed window size-based estimates, normalized cross-correlation based method (operating in spatial domain) as well as the field-based measurements.

2. Study Glaciers

Three glaciers namely South Glacier (SG), Chhota Shigri Glacier (CSG), and Tasman Glacier (TG) (Fig. 1) have been selected based on availability of datasets and variability in terms of glacier size, debris coverage, climatic region, and glacier complexity (Table 1).

Figure 1 comes here.

South Glacier is located in Canada. It is a small glacier of about 4 km long and around 700 m wide. This glacier is totally free of debris. With an average slope of 13°, it lies within the altitude range of 1,970-2,960 m. It is influenced by sub-arctic continental climate. Chhota Shigri Glacier is located in the western Himalayas, India. It is a medium sized glacier about 9 km long with an average width of 800 m. This glacier has mild debris cover. Its average slope is 17° and elevation range lies between 4,050 m and 6,263 m. This glacier is influenced by the Asian monsoon in summer and by the westerlies in winter. Tasman Glacier is located in the Southern Alps, the largest glacier of New Zealand. Extending up to a length of about 25 km with an average width of about 1300 m. The average surface slope of the glacier is 5.4° and the elevation ranges from 3,870 m to 5,500 m. The region is dominated by marine west coast climate. Surrounded by New Zealand's highest peaks, numerous tributary glaciers contribute to this glacier system. Frequent rock avalanches help sustain a relatively thick debris cover on this glacier, which terminates in the proglacial Tasman Lake (Fig. 1c).

Table 1 comes here.

3. Data

To test the proposed approach, only freely available or low-cost SAR and optical remote sensing data covering the study regions have been used. The time periods of satellite datasets were chosen according to the availability of field data measurements. Details of the optical, SAR satellite data and ancillary data such as Digital Elevation Model (DEM), glacier boundaries, and field-based velocity data used for validation are discussed.

3.1 Optical Dataset

The choice of optical image (and constituting bands) to find appropriate window size(s) for feature tracking is bound by the condition that the image should have a similar resolution to that of the SAR data, be cloud free, and close to the end of the ablation season (September for South Glacier and Chhota Shigri; March for Tasman Glacier) to achieve minimum snow cover over glaciers. However, due to the unavailability of any cloud free optical data that covers the South Glacier in the ablation period, data from a different season was used. It is expected that this would affect the accurate determination of the window size due to seasonal snow cover. The details of the optical dataset that was used are listed in Table 2.

Table 2 comes here.

3.2 SAR Dataset

The SAR datasets from Sentinel-1 in Single Look Complex (SLC) format, ENVISAT in SLC format and ALOS PALSAR in Radiometric Terrain Corrected (RTC) format were used to perform maximum likelihood (ML) based glacier feature tracking. It shall be noted that the ALOS PALSAR data is freely available in RTC format and not in SLC. The datasets have been chosen to ascertain the acquisition over same area which is identified by track and frame number. The corresponding details are given in Table 3. Considering that the feature tracking is performed on SAR imagery, it is preferable to use L-band as compared to other bands (C-band and X-band) due to its better radar signal penetration, which adds to correlation between two long-term interval images (Rignot et al., 2001; Nakamura et al., 2007; Strozzi et al., 2006; 2008). However, the

limited availability of freely available L-band ALOS data across the study glaciers has led to the use of C-band as an alternative.

Table 3 comes here.

3.3 Other Datasets

Apart from satellite imagery, other datasets such as Digital Elevation Model (DEM), glacier boundary, and field observations were also used. Freely available Shuttle Radar Topography Mission (SRTM) 1arc second DEM was used to orthorectify the Envisat SAR imagery for Chhota Shigri and Tasman Glacier. However, due to the lack of SRTM over 60° North, the Canadian Digital Elevation Model (CDEM) was used to orthorectify the SAR imagery of South Glacier. Glacier outlines were taken from the latest version of Randolph Glacier Inventory (RGI 6.0). The data used for validation consists of annual glacier velocity measured at different stakes locations over the study glaciers. For South Glacier, the velocity data was obtained from Flowers et al., (2011), which was collected during the years 2005-2010. For Chhota Shigri Glacier, the field measured glacier velocity information was obtained from Azam et al. (2012), which was collected during the year 2009-10. Likewise, for Tasman Glacier, the reference glacier velocity data as reported by Farinotti et al. (2017) and Purdie et al. (2018) was used for validation, which was collected during the years 2000-2011.

4. Methodology

The proposed feature tracking method named as SWIFT (**S**patially varying **WI**ndow based maximum likelihood **F**eature **T**racking; Fig. 2) comprises two stages: i) determination of the spatially varying window size from optical image based on the OBIA concept, and ii) image matching based feature tracking using the maximum likelihood of SAR speckle as similarity measure.

4.1 Automated Determination of Spatially Distributed Window Size

To find the optimum window size distribution for image matching, the concept of OBIA has been used. Using this approach, a glacier is divided into homogeneous regions called segments. This segmentation is done at a scale determined as optimum by the

approach presented in Dragut et al. (2010), where the optimal scale of segmentation was identified from the peak rate of change of local variance (ROC-LV) in the image. Here the segmentation was performed using a bottom-up approach of region-growing segmentation (Dragut et al., 2010), in which, starting from one pixel, the segment grows in size; the growth is defined by the scale that controls the homogeneity of the resulting segments. Once the segment properties exceed the heterogeneity threshold (as determined by the scale), this growth stops. Additional constraints can be provided by giving weight to shape and compactness of the resulting segments. The weights given to the shape factor indirectly signifies how much spectral information should be used. Conversely, the weight given to the compactness factor signifies the degree of compactness of the segments' shape (Definiens Developer, 2007).

Assuming that the glacier features can be of varying shapes, which are rarely compact, the shape and compactness of segments are not considered in the present study, thus giving weight only to the pixel values (also known as digital number) in the optical image. The image segmentation was performed on optical imagery falling in the same season as that of the SAR images to reduce any seasonal disturbances contributing to errors in the feature tracking.

A segmented image contains different shape and size segments. To calculate the window size for image matching, geometric properties like length and width of segments have been utilized in the present study. To avoid complexity, instead of matching 'segments' which are irregular in nature, a simplified square size window was chosen to perform image matching without any major loss in information. The square window, which closely matches the segment's geometry is referred to as the window size (WS). Since the segments may vary in geometry over a glacier, the window size was kept as a spatially varying parameter. The main advantage of having a spatially varying window size(s) over that of a fixed window size is that different sized features can be tracked more accurately, with window size(s) closely corresponding to actual features over a glacier surface.

Figure 2 comes here.

Additionally, a constraint was applied to the window size distribution in which only window sizes less than or equal to the average width of the glacier (W_{avg}) were considered. Window sizes greater than this were discarded to avoid any unrealistic large values. Here, the average width of the glacier was calculated by taking the cross-sectional width at different locations of the glacier's main trunk to approximate the average width of the glacier. Thus, the final window size is calculated as,

$$\text{Window Size (WS)} = \begin{cases} \text{WS} & \text{if WS} < W_{avg} \\ W_{avg} & \text{if WS} > W_{avg} \end{cases} \quad (1)$$

This step should not be interpreted as manual selection, as with the advent of GIS tools, and freely available remote sensing and glacier inventory datasets containing glacier polygons, automated calculation of glacier geometries such as length and width are possible (Pfeffer et al., 2014; James and Carrivick, 2016). Moreover, this window size selection technique is independent of glacier type or its environment setting, thus making it applicable to glaciers in any setting.

4.2 SAR Feature Tracking

A multiplicative speckle model-based SAR feature tracking method was implemented to estimate glacier surface velocities, where images are compared based on maximum likelihood of SAR speckle. Speckle, which is inherently present in every SAR image gives useful information about the glacier surface characteristics. This speckle can be tracked in time-lapse SAR imagery and thus helps estimate glacier flow. Before performing the SAR feature tracking, geometric distortions in SAR images due to side looking viewing geometry were corrected using the DEMs listed in section 3.3.

Assuming that the blocks to be matched between two SAR images X and Y of size m × n share a common region at two annually separated time periods T_1 and T_2 (Fig. 3), the distribution of Maximum Likelihood (ML) estimators was calculated for different candidate shifts between the two images for each block/matching-window. The maximum likelihood estimate (v_{ML}) of velocity v_i was obtained by maximizing the cumulative distribution function (CDF) function (ρ) for each block i according to

$$\rho\left(x_{ij}\middle|y_{ij}, v_i\right), \quad (2)$$

where x_{ij} and y_{ij} are the pixels corresponding to block X and Y respectively. The above function can also be represented in terms of block size by the objective function

$$\sum_{j=1}^{k} \ln y_{ij} + \ln x_{ij} - 2\ln(x_{ij}+y_{ij}) - \frac{\ln x_{ij}}{N}, \quad (3)$$

where k is the total number of pixels in a block and N is the multi-looking factor.

Figure 3 comes here.

Following Debellagilo and Kaab (2010), sub-pixel interpolation has been undertaken to achieve sub-pixel precision of ¼ of a pixel by capturing the displacements smaller than the spatial resolution of the input satellite images. The horizontal displacements were derived from the slant range displacements following Strozzi et al. (2002) and Sanchez-Gamez and Navarro (2017) to facilitate the comparison with ground-based field measurement of horizontal glacier velocity. From the azimuth and slant range displacements, the net horizontal displacement is calculated using the relation

$$\text{Net Displacement} = \sqrt{(R_x\Delta x)^2 + (R_y\Delta y)^2} \quad (4)$$

where R_x and R_y are the pixel spacing in azimuth and slant range directions, Δx and Δy are the displacements in azimuth and slant range directions. The velocities outside the 3×Inter Quartile Range (IQR) have been removed as outliers from the estimates (Fig. 4). The blank patches have been filled using a mean filter where the kernel size is kept the same as the window size distribution. This filtering approach has been chosen to eliminate the subjectivity of choosing a smoothing filter for individual glaciers.

4.3 SWIFT Implementation and Uncertainty Assessment

The proposed method was implemented in MATLAB on a 4.6 GHz Intel® Core i7-8700 CPU of 16GB RAM system. The pre-processing of data was performed on the freely available SentiNel Application Platform (SNAP). Terrain correction was performed for all of the SAR imagery (section 3.2) except the ALOS PALSAR image, which had already been terrain corrected. The geometric co-registration of the SAR dataset has been addressed during DEM assisted co-registration (Nitti et al., 2010; Sanchez-Gamez and Navarro, 2017) in Terrain Correction with an RMSE threshold of 0.3 (of pixel size) during the co-registration. Readers are referred to the SNAP user guide for a detailed description of this process (https://scihub.copernicus.eu/userguide).

Uncertainty in the proposed surface velocity tracking method includes: i) uncertainty due to the spatial resolution of the SAR image pair, and ii) uncertainty due to the co-registration error between these image pairs. The former is dependent upon the spatial resolution of the input SAR images, while the latter is reported as the RMSE obtained after the DEM assisted co-registration. The total uncertainty was calculated using the two above mentioned uncertainties via summation of quadrature method of error propagation

$$\text{Total Uncertainty} = \sqrt{\Delta U_{res}{}^2 + \Delta U_{Co-reg}{}^2} \quad (5)$$

where the two entities ΔU_{res} and ΔU_{Co-reg} represent the uncertainties due to spatial resolution and co-registration respectively and were considered uncorrelated (Anderson 2019).

5 Results

The window size obtained for different study glaciers are presented followed by their overall and zone-wise surface velocity estimates. The method's performance was evaluated using accuracy assessment against the available field measurements and previously reported values of glacier surface velocity. Here, statistical measures such as

the root mean square error (RMSE) and bias were used for performance assessment of the SWIFT method.

5.1 Window Size Determination

A spatially varying window size has been determined for each study glacier according to the proposed method. It was found during image segmentation that the segments sometime merged with areas outside of the glacier due to very low/no contrast between the glacier and its surroundings (Fig. 4). This results in a very large window size, which could be as large as the size of the glacier itself. To control this, a constraint on maximum window size has been applied to all three study glaciers. Consequently, substantial improvement in the estimated velocity was observed for Tasman Glacier. However, for the other two glaciers (South Glacier and Chhota Shigri Glacier) no visible improvements were observed due to the absence of segments merging with the background. The obtained range of window size for each glacier was: 5×5 pixels to 46×46 pixels (South Glacier); 3×3 pixels to 80×80 pixels (Chhota Shigri Glacier) and 15×15 pixels to 120×120 pixels (Tasman Glacier). A general trend was observed where minimum window sizes were obtained near the snout region and near the glacier boundaries, whereas, larger window sizes were observed in the glacier accumulation region.

Figure 4 comes here.

5.2 Glacier Surface Velocity Estimates

South Glacier

Here, the proposed feature tracking approach was implemented for the two time periods viz., 2005-06 and 2014-15. The obtained spatial distribution of the estimated surface velocities for the two time periods are shown in Figs. 5a and b.

Figure 5 comes here.

Following DePaoli and Flowers (2009), the results were evaluated for three zones. The zone-wise and overall error statistics for all three study glaciers are given in Table 4. The overall RMSE of the surface velocity estimates of South Glacier for the

periods 2005-06 and 2014-15 with respect to the glacier-wide stake measurements given by Flowers et al. (2011) were 13.25± 5.28 m/yr and 12.8± 5.28 m/yr, respectively (Table 4). The combined uncertainty is presented as a summation in quadrature which is ± 5.28 m/yr for both study periods being 2005-06 and 2014-15. The overall bias for these periods were 9.5 m/yr and 11 m/yr, respectively (Table 4). For both study periods (2005-06 and 2014-15) overall RMSE values were observed to be very close (Table 4), although the optical data used were of different wavelengths. Specifically, the ASTER band 3 (VNIR) was used for 2005-06 while the Landsat 8 PAN band was used for 2014-15. This shows that the proposed feature tracking approach is robust even when different optical datasets were used.

Table 4 comes here.

Figures 5a and b show the estimated and observed surface velocities along the glacier central flowline. Due to unavailability of field measurements for the same year, the estimated glacier surface velocity was compared with the following year's field observations. Here it is assumed that annual velocity does not change substantially from year to year on this glacier. For both time periods, higher surface velocities were captured in the mid and upper zones of the glacier (Figs. 5a and b), where a surge has been reported earlier (Johnson and Kasper, 1992; DePaoli and Flowers, 2009). However, the lower zone which is nearly dormant has not been represented well for both time periods (2005-06 and 2014-15) as revealed by higher RMSEs in this zone (Table 4: South Glacier). From the spatial distribution of surface velocity estimates (Figs. 5a and b) and the comparative plot of the estimated and observed surface velocities (Figs. 6a and b), it is evident that the surface velocities were substantially overestimated in the lower zone. Here, a high value of deviation from the observed velocity in the surface velocity estimates can be attributed to the limitation of least measurable displacement at present level of sub-pixel precision (¼th of a pixel) which exceeds the actual displacement (~0.5 m).

Figure 6 comes here.

The zonal statistics of the surface velocity estimates for each time period are shown in Fig. 6c. For all the zones, the min-max range was similar for both study

periods. However, from mean surface velocities, it appears that for the year 2014-15 all the zones exhibited almost identical surface velocities, which is not consistent with the reported behaviour of this glacier (Depaoli and Flowers, 2009). One of the possible reasons could be the distribution of window sizes ranging from 5 × 5 pixels to 20 × 20 pixels (Supplementary S1b) which are smaller compared to the window size distribution for period 2005-06, which is 5 × 5 pixels to 46 × 46 pixels (Supplementary S1a). These smaller window sizes (which are dominant in the lower zone) can introduce noise in the velocity estimates (Kanade et al., 1994). Similarly, for the year 2005-06, the upper and middle zones showed higher mean velocities than for the lower zone, as reported by DePaoli and Flowers (2009).

Figure 7 shows the glacier wide statistical distribution of velocity estimates for the period 2005-06 and 2014-15. The 2014-15 estimates show a slight acceleration (~13%) in mean velocity from 2005-06 estimates.

Figure 7 comes here.

Chhota Shigri Glacier

The surface velocity estimates for Chhota Shigri Glacier for the period 2009-10 have also been calculated using the proposed methodology and compared with the field-based velocity measurements. Here the window size distribution has been calculated from the IRS LISS-III imagery of Oct 13, 2009 (Table 2). Figure 8a shows the spatial distribution of estimated surface velocity where higher surface velocities can be seen near the glacier snout. Assuming a direct relationship between surface velocity and glacier ice thickness (Cuffey and Paterson, 2010), the peak velocity estimates in the middle zone shown as circled areas 1 & 2 (Fig. 8a) had maximum glacier ice thickness distribution as reported by Huss and Farinotti (2012). However, the circled area 3 (Fig. 8a) in the lower zone showed a very high surface velocity trend, which is not in agreement with the ice thickness estimates reported by Huss and Farinotti (2012). These high values appear to be an indication of an external contribution (like avalanches/landslide) during the study period, leading to substantial changes over the glacier surface which are reflected as erroneous surface velocity estimates. The presence

of active avalanches/landslide sites (Supplementary S3) in the lower zone has been verified by observations made during visits to the Chhota Shigri Glacier.

Figure 8 comes here.

Figure 8b shows a comparison of surface velocity estimates with field measurements along the central flow line of the glacier. It should be noted that the distance is measured from the snout of the glacier. There is a huge difference in the estimated and observed surface velocity at a distance of 2500-3000 m from the snout (Fig.8b), which also coincides with the circled area 3 in Fig. 8a. The overall RMSE of surface velocity estimates of the Chhota Shigri Glacier (excluding the circled area 3) was 15.32± 3.9 m/yr, whereas the overall bias was 3.2 m/yr (Table 4: Chhota Shigri Glacier). Here, the uncertainty in the surface velocity estimation for this glacier is calculated to be ± 3.9 m/yr.

A number of studies have reported mean surface velocity (annual) of Chhota Shigri Glacier for intermittent periods between 1987 and 2010. The surface velocity estimates obtained by the proposed method agree with this reported trend as shown in Fig. 9. It is also observed that the mean velocity of this glacier has not changed much during these 23 years indicating that the glacier is more or less stable.

Figure 9 comes here.

Figure 8c shows the zone-wise statistics of the surface velocity estimates. The min–max range of the estimated velocities lie within the range of previously reported estimates for this glacier by Gantayat et al. (2017). However, the maximum velocity in the lower zone was high (~80 m/yr) when compared with field values in this zone (~30 m/yr), as shown in Fig. 8b. The possible reason has been discussed earlier in this section pertaining to the circled area 3 (Fig. 8a). The estimated mean velocity in the upper, middle and lower zones are 35 m/yr, 45 m/yr and 32 m/yr respectively (Fig. 8c). The mean of lower zone estimates (32 m/yr) and the middle zone (45 m/yr) were found to be close to the observed velocities in the respective zones (20-35 m/yr in the lower zone; 35-45 m/yr in the middle zone). The upper zone estimates could not be evaluated because of unavailability of field measurement over this zone.

The knowledge of Chhota Shigri Glacier's conditions and flow behaviour gathered from field observations has made it possible to further analyse the directional aspects of the velocity estimates. The direction of surface velocity estimates shows an agreement with the aspect direction (Fig. 10b) along the main trunk of the glacier, which follows Northwest-North-Northeast directions. However, the direction in the tributary in regions I & III (Fig. 10a) was not well captured, which can be attributed to large displacements in these regions due to steep slopes. The directional behaviour of the estimated surface velocities in region II is interesting (Fig. 10a), because it highlights the presence of a number of avalanche-prone cliffs to the Northwest, contributing to apparent periodic glacier flow. There are four sites in region II which are affected by avalanches/landslides (Supplementary S3) as identified from the Google Earth image collections available during the study period. Thus, in region II the dominant direction of the surface velocity is obtained as the Northwest direction instead of the North direction as represented by the aspect map (Fig. 10b).

Figure 10 comes here.

Tasman Glacier

The spatial distribution of the estimated surface velocities for the period 2005–06 and 2007–08 are shown in Fig. 11. A smooth transition of glacier velocity is observed from the glacier head to the terminus. However, a few noisy patches near the confluence zone (Figs. 11a–b) can be easily seen, indicating mismatches in the estimated and observed values.

Figure 11 comes here.

The estimated surface velocity values were compared with both i) point-wise field-based surface velocity measurements collected by Purdie et al., (2018) during 2007-09 (Fig. 11), and ii) spatially distributed decadal average surface velocity map (Fig. 12) for the period 2000-2011 (Farinotti et al., 2017), which was derived from field measurements and remote sensing-based estimates (Purdie et al., 2018).

The difference between the derived surface velocity estimates for the periods 2005-2006 and 2007-2008, and the spatially distributed decadal surface velocity

estimates (considered as reference) given by Farinotti et al. (2017), are shown in Fig. 12a-c. Moreover, Fig. 12a shows the difference map for the period 2005-06 where the velocity was estimated without limiting the window size. After limiting the maximum window size, the velocity estimates for the same period were compared with the reference velocity map and the resulting difference map shown in Fig. 12b.

Figure 12 comes here.

Setting a limit on maximum window size showed substantial improvement in the velocity estimates as the velocity difference reduced from ~300 m/yr to ~150 m/yr (Figs. 12a and b). Therefore, for the period 2007-08 the surface velocities were estimated only after limiting the maximum window size. The corresponding difference map with reference velocity is shown in Fig. 12c, where estimates for 2007-08 showed a smoother transition between the different velocity ranges, as expected from an ideal glacier flow. This could be due to higher signal penetration of L-band (used for 2007-08 estimates), which gives less noisy velocity estimates when compared to C-band (used for period 2005-06). It should be noted that the snow wetness can affect L-band penetration capabilities, but this aspect could not be explored in this study as proper information on the snow conditions are not available.

A point-wise comparison of the proposed method with field measurements (Purdie et al., 2018) was conducted as shown in Fig. 13. For the study period 2005-06, large deviation from field data was observed in the lower zone, which also represents the debris cover region with erroneous patches 1, 2 & 3 (Fig .11a). The estimates for period 2007-08 were consistently closer (for lower as well as middle zones) to the field measurements.

Figure 13 comes here.

The overall RMSE for Tasman Glacier (Table 4) during 2005-06 and 2007-08 was 71 m/yr and 67.1 m/yr respectively. Overall, the bias of the velocity estimates for period 2005-06 and 2007-08 was 28.81±5.14 m/yr and 13.14±0.14 m/yr respectively (Table 4). The uncertainty in velocity estimates for the period 2005-06 was ±5.14 m/yr. For the period 2007-08 the uncertainty in the velocity estimates was ±0.14 m/yr. The

uncertainty for this period was very low because only the uncertainty due to spatial resolution of SAR imagery has been reported, while the uncertainty due to co-registration error could not be determined. It is because the error in co-registration could not be calculated for the already processed SAR image pair wherein the DEM based co-registration was not performed. Also, Ground Control Points (GCPs) were not available to perform additional processing.

Figure 14 comes here.

The zone-wise statistics of the surface velocity estimates are shown in Fig. 14. In each zone, estimates for the period 2005-06 showed a higher range of velocity (min-max), pertaining to the presence of noise (Fig. 14b). The mean in the lower zone (also the debris covered zone) was well represented for the periods 2005-06 and 2007-08. In this zone, the mean estimates for both periods were closer to observed velocity (Table 4: Tasman Glacier), showing the reduced effect of the erroneouos patches (Fig. 11a and b).

5.3 Validation over Stable Terrain

The estimated velocities were validated over stable ice-free ground (outside each glacier) where the velocity is expected to be zero, as done by earlier studies (Eg. Altena et al., 2019; Sattar et al., 2019). The estimated displacements at selected stable points near each study glacier are summarized in Table 5. The median 95% confidence interval was found to be 3.7 m/yr (for all three study glaciers combined) in stable areas. This value is slightly higher than the reported value (mean velocity over stable terrain < 3m) for the western Himalayan glacier regions by Das and Sharma (2021). However, the average displacement obtained in the stable area was well within the acceptable limits considering the range of velocity for the study glaciers, which varies between ~30 and 150 m/yr. The displacements obtained in the stable area can be due to errors present in 1) the feature tracking method or 2) ionospheric errors in the input dataset (Yan et al., 2013). The datasets used in the study vary in terms of sensors and processing quality and thus may exhibit different levels of ionospheric errors associated with them. The highest estimates were observed for Tasman Glacier for the period 2007-08 (4.4 m/yr) where the L-band SAR data was used, which is expected to contribute to errors due to higher sensitivity to ionospheric errors (Meyer and Nicoll, 2008).

Table 5 comes here.

6 Discussion

The effect of optical data timestamp on the window size estimates is discussed first followed by the effect due to different SAR datasets on the estimated velocities. These discussions are based purely on the variety of datasets that were available for the study. Next, the spatially varying nature of SWIFT is discussed as assessed against the spatially fixed window size-based estimates. Lastly, the performance evaluation of SWIFT against Normalized Cross Correlation (NCC) method is presented.

6.1 Effect of Optical Data Timestamp on Window Size Estimates

The proposed SWIFT method uses optical data to estimate the window size distribution. Sometimes due to cloud cover, using an optical image of the desired acquisition period may not be possible. Thus, to investigate alternatives, a comparison was made between the window size distributions obtained from optical images acquired at two different time periods (T_1 & T_2) a year apart. For illustration purpose, the window size distribution obtained for the Chhota Shigri Glacier from the images acquired in the 2009 and 2010 ablation periods are shown in Figs. 15a-b. The results obtained indicate a similar trend of window size distribution for both images. This portrays that the window size from the same season's imagery (a year apart) leads to a similar window size distribution. Furthermore, the corresponding velocity from these window sizes was found to be similar (Fig. 15c). Based on this analysis it is evident that choosing either T_1 or T_2 optical imagery did not have a substantial effect on the velocity estimates. Similar observations were seen for South Glacier when two optical images of the ablation season separated a year apart was tested. Such analysis could not be performed for Tasman Glacier, since only one optical image was available during the study period.

From Figs. 15a and b, it is also observed that for a medium sized glacier such as the Chhota Shigri Glacier, the window size barely crosses 80 × 80 pixels, which gives an idea of the range of window sizes that can be used for medium sized glaciers. However, this observation needs to be verified by extensive testing of the method. Similar results were obtained for South Glacier (Supplementary S2), supporting the similarity in window size distribution from two optical images of different time. This

analysis could not be performed for Tasman Glacier, since only one optical image was available during the study period.

It was observed that choosing an optical image far from the study period introduced errors in the estimates. A substantial decrease in feature tracking performance (for South Glacier) was observed when the window size for a given period was used to estimate the surface velocities for other time periods, specifically when the temporal distance between those time periods was large. For example, using the window sizes obtained from images of 2005-06 for estimating velocities for the period 2014-15 led to substantial degradation in feature tracking performance. This could be due to the substantial changes in glacier surface conditions during this ten-year period, which is reflected in the different window size distribution for these periods (Supplementary S1). This observation suggests that optical images selected for window size determination, should not be far from the study period. This is particularly important if the glacier surface conditions have changed notably between the study period and the selected time stamp of the optical image, as this can degrade the performance of the proposed feature tracking approach. In general, this is not the case when the temporal separation between the optical images (used for window size estimation) and the SAR images (used for feature tracking) is approximately one year, provided there is negligible change in surface conditions. This finding implies that the choice of the time stamp of the optical image is a function of the change in glacier surface conditions.

Figure 15 comes here.

6.2 Effect of SAR Dataset

Use of a common optical image to estimate velocity of the Tasman glacier for both study periods (2005-06 and 2007-08) has allowed investigation on the effect of different SAR data on the performance of SWIFT. The Tasman Glacier is a relatively smooth (less steep) glacier whose surface velocity has been reported to have no measurable change during 2002-05 (Herman et al., 2011). Assuming that during 2005-2008 there were no substantial changes in glacier flow behaviour, the effect of SAR wavelength on the feature tracking was investigated. It is interesting to see that L-band (Fig. 13:

Estimated 2007-08), which has more penetration through the glacier, captured the surface velocity more accurately as compared to the C-band based estimates (Fig. 13: Estimated 2005-06). A higher value of RMSE and bias in the C-band estimates can be attributed to the sensitivity of C-band to surface roughness. The effect of SAR polarization could not be studied due to unavailability of different polarization data in L- and C-band products for the study period (Table 3).

6.3 Comparison with Spatially Fixed Window Size

To investigate any possible improvement due to a spatially varying window size, the performance of the proposed SWIFT method was compared with the same ML-based feature tracking method but implemented with a spatially fixed window size (SFWS). For this purpose, the same SAR data pairs (Table 3) have been used. For the simulations using a spatially fixed window size, standard window sizes of different dimensions such as 32 pixels × 32 pixels, 64 pixels × 64 pixels and 128 pixels × 128 pixels) have been tested. It was observed that the window size of 128 pixels × 128 pixels gave higher errors (in comparison to smaller window sizes) in the estimated velocity, especially for South Glacier and Chhota Shigri Glacier. The obtained results indicate that feature tracking with spatially varying window size (ie. SWIFT) performed consistently better in comparison to SFWS based simulations in all three zones of all three study glaciers (Fig. 16).

Figure 16 comes here.

6.4 Performance Evaluation Against NCC

The performance of the SWIFT method has been compared with the cross-correlation-based method that has a spatially invariable window size. The Normalized Cross Correlation (NCC) method was chosen for the comparison since it is most widely used for glacier surface velocity estimations (Bhambri et al., 2017; Jawak et al., 2018; Van Wyk De Vries and Wickert 2021). Moreover, both the methods perform image-matching in the spatial domain. The latter is based on the normalized cross-correlation (NCC) image analysis that was implemented in Correlation Image Analysis Software (Heid and Kaab, 2012). The same SAR data pairs (Table 3) have been used in both methods. Since the proposed SWIFT method uses a spatially varying window size for

image matching, the NCC-derived estimates have been calculated for different standard window sizes (32 × 32, 64 × 64, and 128 × 128 pixels) and subsequently compared with the proposed method. The search window size was maintained at 100 × 100 pixels for both the NCC and the proposed method. Any gaps in NCC estimates were filled using the Inverse Distance Weighted (IDW) interpolation. This analysis was performed for all three study glaciers for the available dataset (Table 3). Although, the NCC estimates at different window size (32 × 32 pixels, 64 × 64 pixels, and 128 × 128 pixels) have been used for calculations (Supplementary S4), to ease the interpretation only the best performing window size (NCC) for each glacier and the proposed method's estimates are shown in Figs. 17a-c. A summary of zone-wise and overall RMSE of the NCC based approach for the study glaciers is given in Table 6.

Table 6 comes here.

Comparison of the RMSEs from Table 4 and Table 6 indicates that the surface velocity in middle and upper zones for all three study glaciers were estimated more accurately by the proposed approach than the NCC based approach, where the NCC approach tends to fail due to low contrast (increased snow cover) on the glacier surface. However, the NCC estimates outperformed the proposed approach in the lower zone of the South Glacier. Conversely, for Chhota Shigri Glacier the proposed method performed better. For the lower zone of the Tasman Glacier, similar conclusions could not be derived because the RMSEs were calculated from a single stake measurement. Here, the SWIFT method was observed to be sensitive to highly textured areas, especially the lower zone which is a highly textured zone due to debris cover and/or surface melting. This observation is also conveyed in Figs. 17a-c. Overall, when compared with the best results of the NCC method (which requires calibration), the SWIFT approach was in close agreement for the South Glacier and performed better in case of Chhota Shigri Glacier and Tasman Glacier (Table 4 and Table 6).

It is noteworthy that the best window size in the NCC method was different for each glacier (Figs 17(a-c)), which can be obtained only in the presence of field measurements; and it is spatially invariant over the glacier surface. Conversely, the window size used in the proposed approach was automatically identified - it does not

require field measurements - taking the varying nature of the glacier surface features into account. This demonstrates the advantage of the proposed approach over the NCC-based approach.

The processing time for the two methods (NCC and SWIFT) took from several minutes to a few hours. For SWIFT, the processing time varied depending upon glacier size whereas, for NCC, it varied for glacier size as well as the chosen window size.

Figure 17 comes here.

7. Summary and Conclusion

A new method called the spatially-varying-window-based feature tracking (SWIFT) is presented for glacier surface velocity estimation. This method provides flexibility in terms of spatially varying window size, unlike other existing software, where the window size can be varied at different iterations while the window size remains spatially constant. It considers both optical (for window size estimation) and SAR data (feature tracking) to estimate glacier surface velocities. The proposed feature tracking method was tested for three study glaciers located in different parts of the world.

The proposed SWIFT method was evaluated for possible impacts of input data characteristics (such as time stamp of optical imagery and spatial resolution of SAR-optical data pairs) on the estimated glacier surface velocity. Investigations into the effect of time stamp of input optical imagery led to the conclusion that, in the case where optical data is not available during the study period, choosing an alternate data is possible. Choosing an optical data of the same season which is a year apart is feasible provided negligible changes in the glacier surface.

When compared with spatially fixed window size-based feature tracking, the proposed spatially varying method gave better velocity estimates for each of the three study glaciers. Furthermore, comparison of zone-wise velocity estimates of the study glaciers obtained from the proposed SWIFT method with the normalized cross correlation method revealed improvements due to the proposed method. This analysis revealed a better performance of the SWIFT approach in the middle and upper zones of

the study glaciers. However, in the lower zone, the SWIFT method gave relatively higher RMSEs when compared to the best performing NCC (CIAS) estimates. One of the key contributions of the present study is the automated estimation (no calibration of window size required) and the spatially variable nature of the window size(s). Similar to other NCC based methods, large intra annual changes on the glacier surface and co-registration errors are the factors that limit the accuracy of this feature tracking approach. Nevertheless, the proposed glacier feature tacking method holds potential for feature tracking in glaciers with no prior field information available.

The current version of the proposed SWIFT method focuses on minimizing manual involvement while estimating glacier velocity rather than increasing computational efficiency. However, computationally, this tracking approach does not pose any severe limitations and it is dependent upon the size of the glacier and the window size generated. For example, with a 4.6 GHz Intel® Core i7- 8700 CPU of 16GB RAM, the total Central Processing Unit (CPU) time (applicable to both parallel and serial processing) may vary from several minute to a few hours because of the spatially varying window size and glacier size. In this study, the proposed method has been tested for three study glaciers (valley type glaciers) and should be rigorously tested for glaciers with varying level of debris cover and glaciers in the polar region such as marine terminating glaciers. Such extensive testing will help us in assessing the potential of global scale applicability of the developed glacier surface velocity estimation method.

Acknowledgements

Authors thank both the anonymous reviewers for their comments, which helped us to improve the quality of the manuscript. We acknowledge the support provided by the IITB-Monash Research Academy to engage IIT Bombay and Monash University in carrying out this work. We are thankful to the European Space Agency and JAXA for providing freely accessible SAR datasets. We would like to thank USGS and ISRO for providing optical datasets used in this study. Last but not the least, we would like to

acknowledge Dr. Farooq Azam and Dr. Gwenn Flowers for providing data and useful information about the study glaciers i.e., Chhota Shigri and South Glacier respectively.

Data Availability Statement:

Satellite data that were used in the study are freely accessible from the mentioned repositories. We do not own the sharing rights for the field data used. However, they can be obtained from the relevant publications cited in the article.

References

Ahn Y, Howat IM. 2011. Efficient Automated Glacier Surface Velocity Measurement from Repeat Images Using Multi-Image/Multichip and Null Exclusion Feature Tracking. *IEEE Trans Geosci Remote Sensing*. 49(8):2838–2846.

Altena B, Scambos T, Fahnestock M, Kääb A. 2019. Extracting recent short-term glacier velocity evolution over southern Alaska and the Yukon from a large collection of Landsat data. *Cryosphere*. 13(3):795–814.

Andersen ML, Stenseng L, Skourup H, Colgan W, Khan SA, Kristensen SS, Andersen SB, Box JE, Ahlstrøm AP, Fettweis X, et al. 2015. Basin-scale partitioning of Greenland ice sheet mass balance components (2007–2011). *Earth Planet Sci Lett*. 409:89–95.

Anderson SW. 2019. Uncertainty in quantitative analyses of topographic change: error propagation and the role of thresholding. *Earth Surf Process Landf.* 44(5):1015–1033.

Azam MF, Wagnon P, Ramanathan A, Vincent C, Sharma P, Arnaud Y, Linda A, Pottakkal JG, Chevallier P, Singh VB, et al. 2012. From balance to imbalance: a shift in the dynamic behaviour of Chhota Shigri glacier, western Himalaya, India. *J Glaciol.* 58(208):315–324.

Bhambri R, Hewitt K, Kawishwar P, Pratap B. 2017. Surge-type and surge-modified glaciers in the Karakoram. *Sci Rep.* 7(1).

Blaschke T. 2010. Object based image analysis for remote sensing. *ISPRS J Photogramm Remote Sens.* 65(1):2–16.

Chen L-C, Papandreou G, Kokkinos I, Murphy K, Yuille AL. 2018. DeepLab: Semantic Image Segmentation with Deep Convolutional Nets, Atrous Convolution, and Fully Connected CRFs. *IEEE Trans Pattern Anal Mach Intell*. 40(4):834–848.

Chen G, Weng Q, Hay GJ, He Y. 2018. Geographic object-based image analysis (GEOBIA): emerging trends and future opportunities. *GIsci Remote Sens.* 55(2):159–182.

Ciappa A, Pietranera L, Battazza F. 2010. Perito Moreno Glacier (Argentina) flow estimation by COSMO SkyMed sequence of high-resolution SAR-X imagery. *Remote Sens Environ*. 114(9):2088–2096.

Cuffey KM, W S B Paterson. 2010. The physics of glaciers. Amsterdam: Butterworth-Heinemann, Cop.

Das S, Sharma MC. 2021. Glacier surface velocities in the Jankar Chhu Watershed, western Himalaya, India: Study using Landsat time series data (1992–2020). *Remote Sens Appl: Soc Environ.* 24:100615.

Debella-Gilo M, Kääb A. 2011. Sub-pixel precision image matching for measuring surface displacements on mass movements using normalized cross-correlation. *Remote Sens Environ*. 115(1):130–142.

Deledalle C-A, Denis L, Tupin F. 2011. NL-InSAR: Nonlocal Interferogram Estimation. *IEEE Trans Geosci Remote Sens.* 49(4):1441–1452.

Dehecq A, Gourmelen N, Gardner AS, Brun F, Goldberg D, Nienow PW, Berthier E, Vincent C, Wagnon P, Trouvé E. 2019. Twenty-first century glacier slowdown driven by mass loss in High Mountain Asia. *Nat Geosci.* 12(1):22–27.

Developer D. 2007. Definiens AG, Munich, Germany.

De Paoli L, Flowers GE. 2009. Dynamics of a small surge-type glacier using one-dimensional geophysical inversion. *J Glaciol.* 55(194):1101–1112.

Dobhal DP, Kumar S, Mundepi AK. 1995. Morphology and glacier dynamics studies in monsoon–arid transition zone: an example from Chhota Shigri Glacier, Himachal-Himalaya, India. *Curr Sci.* 936-944.

Drăguţ L, Tiede D, Levick SR. 2010. ESP: a tool to estimate scale parameter for multiresolution image segmentation of remotely sensed data. *Int J Geogr Inf Syst.* 24(6):859–871.

Derauw D. 1999. DInSAR and coherence tracking applied to glaciology: The example of Shirase Glacier. In Proc. FRINGE. Vol. 99.

Erten E, Reigber A, Hellwich O, Prats P. 2009. Glacier Velocity Monitoring by Maximum Likelihood Texture Tracking. *IEEE Trans Geosci Remote Sens*. 47(2):394–405.

Farinotti D, Brinkerhoff DJ, Clarke GKC, Fürst JJ, Frey H, Gantayat P, Gillet-Chaulet F, Girard C, Huss M, Leclercq PW, et al. 2017. How accurate are estimates of glacier ice thickness? Results from ITMIX, the Ice Thickness Models Intercomparison eXperiment. *Cryosphere*. 11(2):949–970.

Fahnestock M, Scambos T, Moon T, Gardner A, Haran T, Klinger M. 2016. Rapid large-area mapping of ice flow using Landsat 8. *Remote Sens Environ*. 185:84–94.

Flowers GE, Roux N, Pimentel S, Schoof CG. 2011. Present dynamics and future prognosis of a slowly surging glacier. *Cryosphere*. 5(1):299–313.

Gantayat P, Kulkarni AV, Srinivasan J, Schmeits MJ. 2017. Numerical modelling of past retreat and future evolution of Chhota Shigri glacier in Western Indian Himalaya. *Ann Glaciol*. 58(75pt2):136–144.

Heid T, Kääb A. 2012. Evaluation of existing image matching methods for deriving glacier surface displacements globally from optical satellite imagery. *Remote Sens Environ*. 118:339–355.

Herman F, Anderson B, Leprince S. 2011. Mountain glacier velocity variation during a retreat/advance cycle quantified using sub-pixel analysis of ASTER images. *J Glaciol*. 57(202):197–207.

Huang L, Li Z. 2011. Comparison of SAR and optical data in deriving glacier velocity with feature tracking. *Int J Remote Sens*. 32(10):2681–2698.

Huss M, Farinotti D. 2012. Distributed ice thickness and volume of all glaciers around the globe. *J Geophys Res Earth Surf*. 117(F4)

James WHM, Carrivick JL. 2016. Automated modelling of spatially-distributed glacier ice thickness and volume. *Comput Geosci*. 92:90–103.

Jawak SD, Kumar S, Luis AJ, Bartanwala M, Tummala S, Pandey AC. 2018. Evaluation of geospatial tools for generating accurate glacier velocity maps from optical remote sensing data. In Multidisciplinary Digital Publishing Institute Proceedings. Vol. 2(7), 341.

Johnson PG, Kasper JN. 1992. The Development of an Ice-Dammed Lake: The Contemporary and Older Sedimentary Record. *Arct Antarct Alp Res*. 24(4):304.

Joughin I, Smith BE, Howat IM, Scambos T, Moon T. 2010. Greenland flow variability from ice-sheet-wide velocity mapping. *J Glaciol*. 56(197):415–430.

Kääb A, Vollmer M. 2000. Surface geometry, thickness changes and flow fields on creeping mountain permafrost: automatic extraction by digital image analysis. *Permafr Periglac Process*. 11(4), 315-326.

Kääb A, Huggel C, Paul F, Wessels R, Raup B, Kieffer H, Kargel J. 2002. Glacier monitoring from ASTER imagery: accuracy and applications. In Proceedings of EARSeL-LISSIG-workshop observing our cryosphere from space. Vol 2, 43-53.

Kanade T, Okutomi M. 1994. A stereo matching algorithm with an adaptive window: theory and experiment. *IEEE Trans Pattern Anal Mach Intell.* 16(9):920–932.

Kumar V, Venkataramana G, Høgda KA. 2011. Glacier surface velocity estimation using SAR interferometry technique applying ascending and descending passes in Himalayas. *Int J Appl Earth Obs Geoinf.* 13(4):545–551.

Kumari S, Ramsankaran RAAJ, Walker JP. 2019. Impact of Window Size in Remote Sensing Based Glacier Feature Tracking–a Study on Chhota Shigri Glacier, Western Himalayas, India. In IGARSS 2019-2019 IEEE International Geoscience and Remote Sensing Symposium. p. 4175-4178.

Mcnabb RW, Hock R, O'Neel S, Rasmussen LA, Ahn Y, Braun M, Conway H, Herreid S, Joughin I, Pfeffer WT, et al. 2012. Using surface velocities to calculate ice thickness and bed topography: a case study at Columbia Glacier, Alaska, USA. *J Glaciol*. 58(212):1151–1164.

Messerli A, Grinsted A. 2015. Image georectification and feature tracking toolbox: ImGRAFT. *Geosci Instrum Methods Data Syst.* 4(1):23–34.

Meyer FJ, Nicoll JB. 2008. Prediction, Detection, and Correction of Faraday Rotation in Full-Polarimetric L-Band SAR Data. *IEEE Trans Geosci Remote Sens*. 46(10):3076–3086.

Nakamura K, Doi K, Shibuya K. 2007. Estimation of seasonal changes in the flow of Shirase Glacier using JERS-1/SAR image correlation. *Polar Sci.* 1(2-4):73–83.

Nitti DO, Hanssen RF, Refice A, Bovenga F, Nutricato R. 2011. Impact of DEM-Assisted Coregistration on High-Resolution SAR Interferometry. *IEEE Trans Geosci Remote Sens*. 49(3):1127–1143.

Palmer SJ, Shepherd A, Sundal A, Rinnem E, Nienow P. 2010. InSAR observations of ice elevation and velocity fluctuations at the Flade Isblink ice cap, eastern North Greenland. *J Geophys Res*. 115(F4).

Patel A, Dharpure JK, Snehmani, Ganju A. 2017. Estimating surface ice velocity on Chhota Shigri glacier from satellite data using Particle Image Velocimetry (PIV) technique. *Geocarto Int*. 34(4):335–347.

Pfeffer WT, Arendt AA, Bliss A, Bolch T, Cogley JG, Gardner AS, Hagen J-O, Hock R, Kaser G, Kienholz C, et al. 2014. The Randolph Glacier Inventory: a globally complete inventory of glaciers. *J Glaciol*. 60(221):537–552.

Pritchard H, Murray T, Luckman A, Strozzi T, Barr S. 2005. Glacier surge dynamics of Sortebræ, east Greenland, from synthetic aperture radar feature tracking. *J Geophys. Res Earth Surf*. 110(F3).

Purdie H, Anderson B, Mackintosh A, Lawson W. 2018. Revisiting glaciological measurements on Haupapa/Tasman Glacier, New Zealand, in a contemporary context. *Geogr Ann A: Phys Geogr*. 100(4):351–369.

Riveros N, Euillades L, Euillades P, Moreiras S, Balbarani S. 2013. Offset tracking procedure applied to high resolution SAR data on Viedma Glacier, Patagonian Andes, Argentina. *Adv Geosci*. 35:7–13.

Rignot E, Echelmeyer K, Krabill W. 2001. Penetration depth of interferometric synthetic-aperture radar signals in snow and ice. *Geophys Res Lett*. 28(18):3501–3504.

Ruan Z, Guo H, Liu G, Yan S. 2013. Glacier surface velocity estimation in the West Kunlun Mountain range from L-band ALOS/PALSAR images using modified synthetic aperture radar offset-tracking procedure. *J Appl Remote Sens*. 8(1):084595.

Sánchez-Gámez P, Navarro FJ. 2017. Glacier surface velocity retrieval using D-InSAR and offset tracking techniques applied to ascending and descending passes of Sentinel-1 data for southern Ellesmere ice caps, Canadian Arctic. *Remote Sens.* 9(5):442.

Sattar A, Goswami A, Kulkarni AV, Das P. 2019. Glacier-Surface Velocity Derived Ice Volume and Retreat Assessment in the Dhauliganga Basin, Central Himalaya – A Remote Sensing and Modeling Based Approach. *Front Earth Sci*. 7.

Scambos TA, Dutkiewicz MJ, Wilson JC, Bindschadler RA. 1992. Application of image cross-correlation to the measurement of glacier velocity using satellite image data. *Remote Sens Environ.* 42(3):177–186.

Scherler D, Leprince S, Strecker MR. 2008. Glacier-surface velocities in alpine terrain from optical satellite imagery—Accuracy improvement and quality assessment. *Remote Sens Environ.* 112(10):3806–3819.

Schubert A, Faes A, Kääb A, Meier E. 2013. Glacier surface velocity estimation using repeat TerraSAR-X images: Wavelet- vs. correlation-based image matching. *ISPRS J Photogramm Remote Sens*. 82:49–62.

Short NH, Gray AL. 2005. Glacier dynamics in the Canadian High Arctic from RADARSAT-1 speckle tracking. *Can J Remote Sens*. 31(3):225–239.

Strozzi T, Luckman A, Murray T, Wegmuller U, Werner CL. 2002. Glacier motion estimation using SAR offset-tracking procedures. *IEEE Trans Geosci Remote Sens*. 40(11):2384–2391.

Strozzi T, Wiesmann A, Sharov A, Kouraev A, Wegmuller U, Werner C. 2006. July. Capabilities of L-band SAR data for arctic glacier motion estimation. In 2006 IEEE International Symposium on Geoscience and Remote Sensing. 3816-3819.

Strozzi T, Kouraev A, Wiesmann A, Wegmüller U, Sharov A, Werner C. 2008. Estimation of Arctic glacier motion with satellite L-band SAR data. *Remote Sens Environ*. 112(3):636–645.

Tiwari R, Gupta RP, Arora MK. 2014. Estimation of surface ice velocity of Chhota-Shigri glacier using sub-pixel ASTER image correlation. *Curr Sci*. 853-859.

Tong X, Liu S, Li R, Xie H, Liu S, Qiao G, Feng T, Tian Y, Ye Z. 2018. Multi-track extraction of two-dimensional surface velocity by the combined use of differential and multiple-aperture InSAR in the Amery Ice Shelf, East Antarctica. *Remote Sens Environ*. 204:122–137.

Turrin J, Forster RR, Larsen C, Sauber J. 2013. The propagation of a surge front on Bering Glacier, Alaska, 2001–2011. *Ann Glaciol*. 54(63):221–228.

Van Wyk de Vries M, Wickert AD. 2021. Glacier Image Velocimetry: an open-source toolbox for easy and rapid calculation of high-resolution glacier velocity fields. *Cryosphere*. 15(4):2115–2132.

Yan S, Guo H, Liu G, Ruan Z. 2013. Mountain glacier displacement estimation using a DEM-assisted offset tracking method with ALOS/PALSAR data. *Remote Sens Lett*. 4(5):494–503.

Yellala A, Kumar V, Høgda KA. 2019. Bara Shigri and Chhota Shigri glacier velocity estimation in western Himalaya using Sentinel-1 SAR data. *Int J Remote Sens*. 40(15):5861–5874.

Table 1. Details of the study glaciers

Glacier	**Location**	**Central Lat/Long**	**Area**	**Debris Coverage**	**Orientation**	**Glacier Complexity**
South Glacier	Canada	60.88° N / 139.12° W	5.3 km^2	No	West	Simple
Chhota Shigri	India	32.24° N / 77.51° E	15 km^2	Yes (~10%)	North	Compound
Tasman Glacier	New Zealand	32.75° N / 77.33° E	101 km^2	Yes (~45%)	South	Compound

Table 1. Details of the optical dataset used for the study.

Satellite & (Sensor)	**Date**	**Path/Row**	**Band No (Spectral Region)**	**Spatial Resolution**	**Glacier**
Terra (ASTER)	Mar 02, 2006	204/717	VNIR 3***** (0.76 - 0.86 µm)	15 m	South Glacier
Landsat 8 (OLI)	Aug 29, 2013	061/017	PAN 8 (0.5 - 0.68 µm)	15 m	South Glacier
Landsat 8 (OLI)	Nov 20, 2014	061/017	PAN 8 (0.5 - 0.68 µm)	15 m	South Glacier
IRS P6 (LISS-III)	Oct 13, 2009 Oct 08, 2010	095/048	VNIR 2 (0.52 - 0.59 µm) 3 (0.62 - 0.68 µm) 4 (0.77 - 0.86 µm) SWIR 5 (1.55 - 1.70 µm)	24 m	Chhota Shigri
Terra (ASTER)	Jan 24, 2006	223/604	VNIR 1 (0.52 - 0.60 µm) 2 (0.63 - 0.69 µm) 3 (0.76 - 0.86 µm)	15 m	Tasman Glacier

Table 2. Details of SAR image pairs used for feature tracking in the study glaciers.

Satellite	Time 1	Time 2	Polarization	Pass	Track	Frame	Resolution (m)	Glacier
Envisat (C-band)	Oct 29, 2005	Dec 23, 2006	VV	Dsc	568	436	5 x 20 m	South Glacier
Sentinel 1 (C-band)	Oct 14, 2014	Oct 09, 2015	VV	Asc	5465	53658	5 x 20 m	South Glacier
Envisat (C-band)	Sep 17, 2009	Sep 02, 2010	VV	Dsc	334	2961	5 x 20 m	Chhota Shigri
Envisat (C-band)	Apr 23, 2005	Mar 04, 2006	VV	Dsc	324	545	5 x 20 m	Tasman Glacier
ALOS PALSAR (L-band)	Feb 07, 2007	Mar 27, 2008	HH	Dsc	456	2344	12.5 m	Tasman Glacier

Table 4. Summary of zone wise RMSE of the proposed feature tracking approach for all three study glaciers. The overall RMSE and bias is also presented for each study period. The different zones are shown in Figures. 1(a-c).

Glacier	Period	Lower Zone	Mid Zone	Upper Zone	Overall	
		RMSE (m/yr)			RMSE (m/yr)	Bias (m/yr)
South Glacier	2005-06	16	8	12.2	13.25	9.5
	2014-15	19	7	11.7	12.8	11
Chhota Shigri	2009-10	11.4	16.9	-	15.32	3.2
Tasman Glacier	2005-06	148.8*	41	-	71	28.81
	2007-08	48.1*	70	-	67.1	13.14

*RMSE has been calculated from one stake measurement.

Table 5. Estimated displacements for each study glacier over stable region.

Glacier	Study Period	Estimated velocity in stable areas (at 95% confidence interval) in m/yr
South Glacier	2005-06	2.4
	2014-15	3.9
Chhota Shigri Glacier	2009-10	4.2
Tasman Glacier	2005-06	3.9
	2007-08	4.4

Table 6. Zone wise RMSE of the normalized cross correlation (NCC) based method CIAS (at best performing window size) for the study glaciers.

Glacier	Period	RMSE (NCC) in m/yr			
		Lower Zone	Mid Zone	Upper Zone	Overall
South Glacier	2005-06	5.5	7.3	18.2	9
	2014-15	5.4	14	11	12.8
Chhota Shigri	2009-10	20.5	21	-	20.8
Tasman Glacier	2005-06	2.4*	115.8	-	105
	2007-08	2.9*	175.9	-	160

*
RMSE has been calculated from one stake measurement.

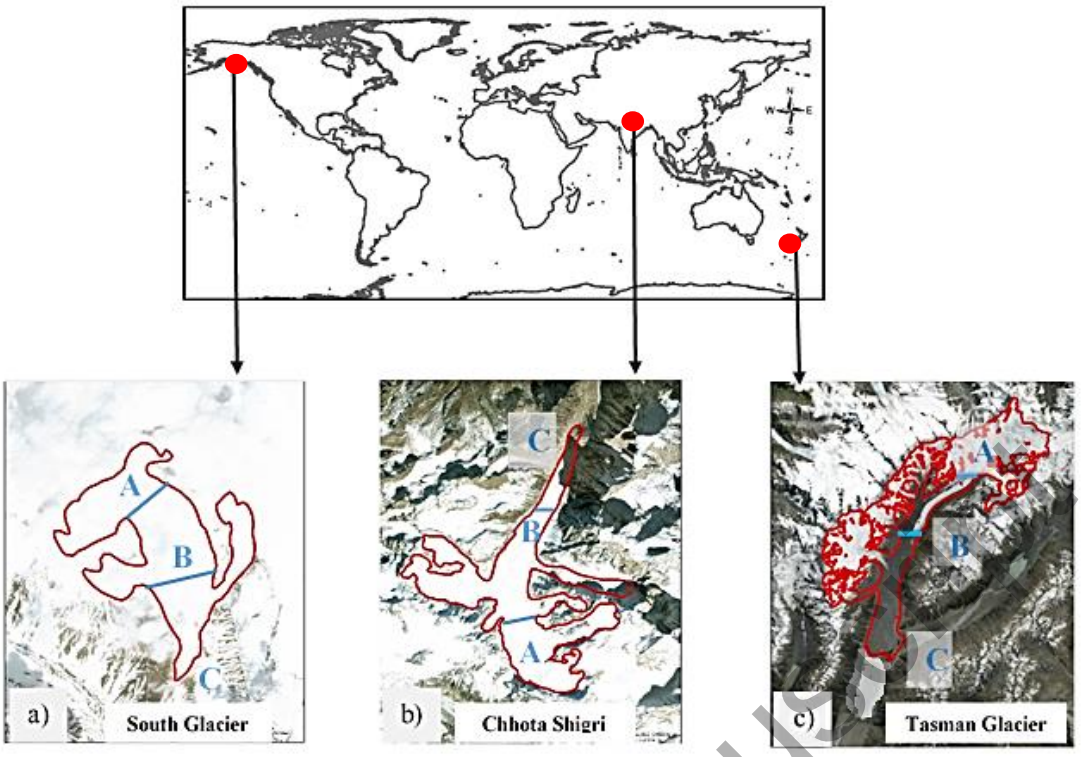

Figure 1. Locations of the three study glaciers (not to scale): a. South Glacier (Canada), b. Chhota Shigri (India), and c. Tasman Glacier (New Zealand). Different zones are shown where A represents the average equilibrium line altitude (ELA) and the region above A represents the upper zone (accumulation zone), the region between A and B represents the middle zone (upper ablation area) and the region between B and C represents the lower zone (lower ablation area) of the glacier.

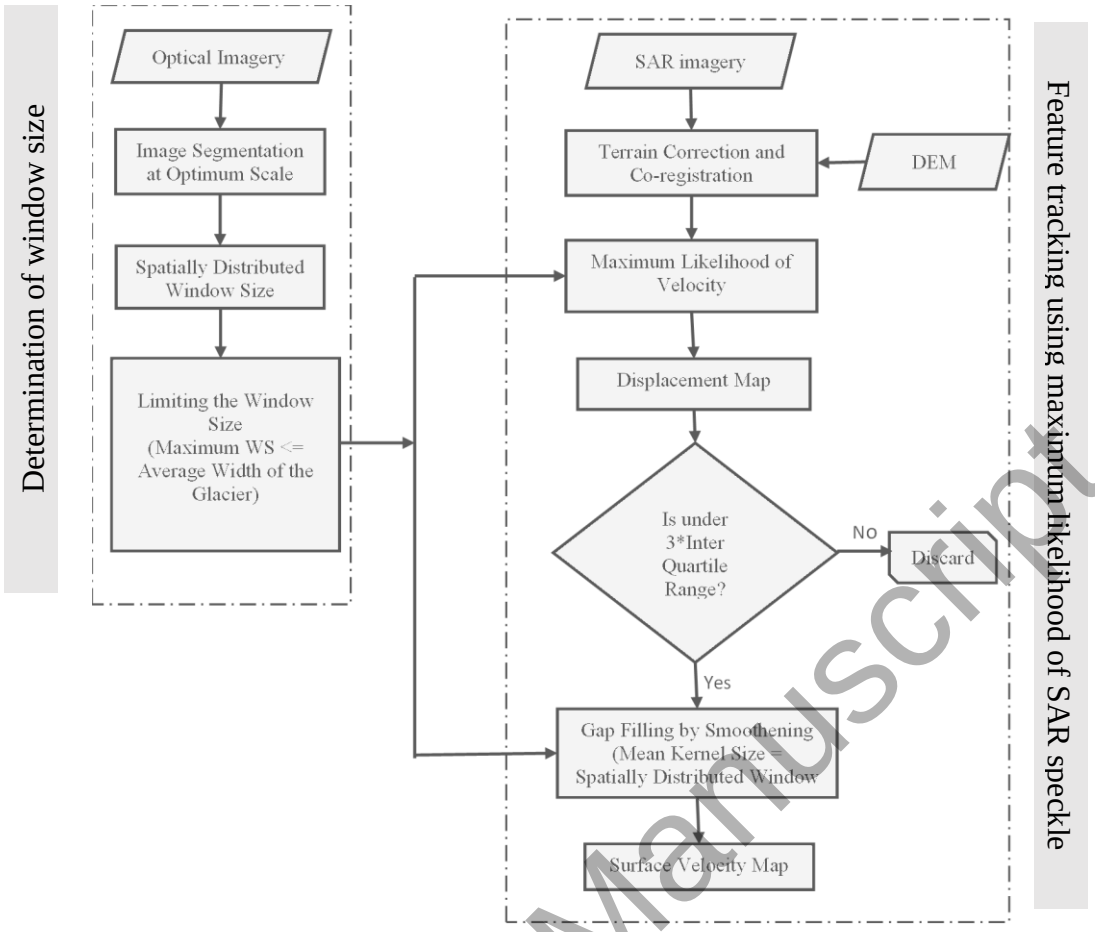

Figure 2. Proposed feature tracking algorithm Spatially varying WIndow based maximum likelihood Feature Tracking (SWIFT) for glacier surface velocity estimations using optical and SAR imagery.

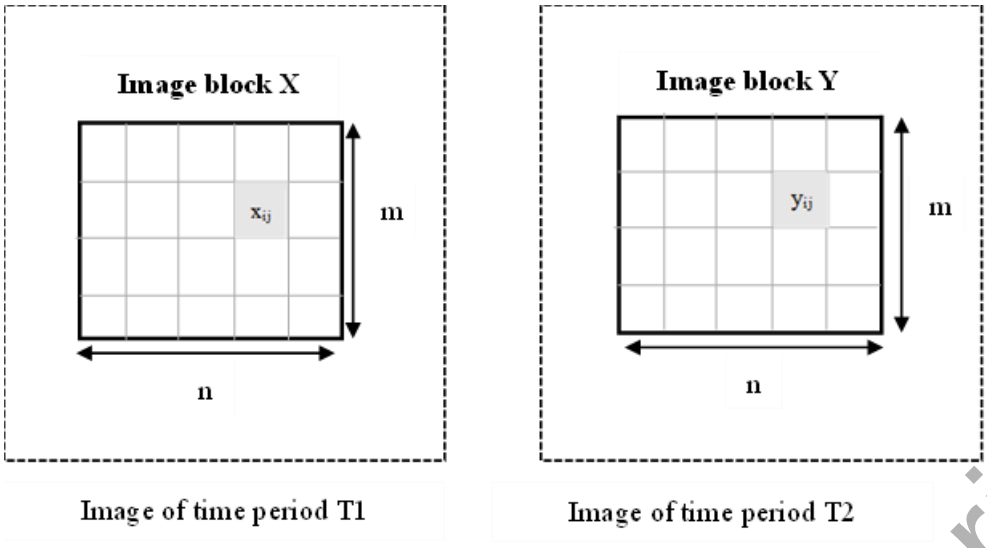

Figure 3. Schematic of image blocks (**X** and **Y**) from two time periods T1 and T2 used in image matching.

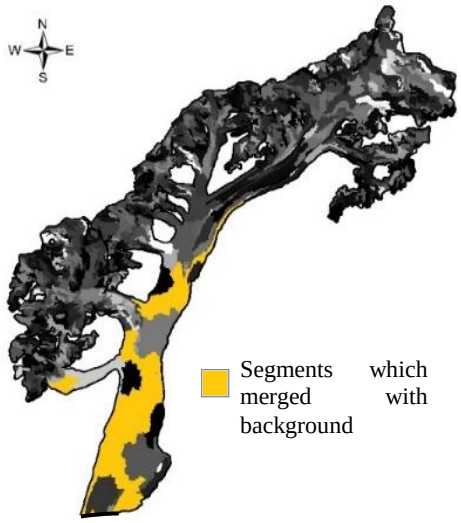

Figure 4. Segmented image of the Tasman Glacier using ASTER (band 1-3). The highlighted segments in yellow are those inside the glacier boundary which merged with a large segment outside the glacier area.

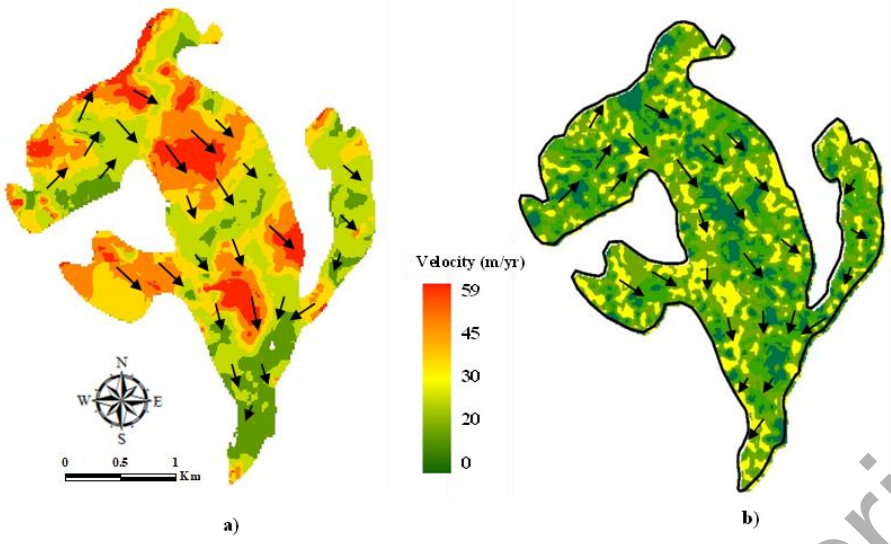

Figure 5. Spatial distribution of the estimated surface velocity values of South Glacier a) for 2005-06 and b) for 2014-15. The arrows show the direction of estimated velocity and the length shows the magnitude of velocity.

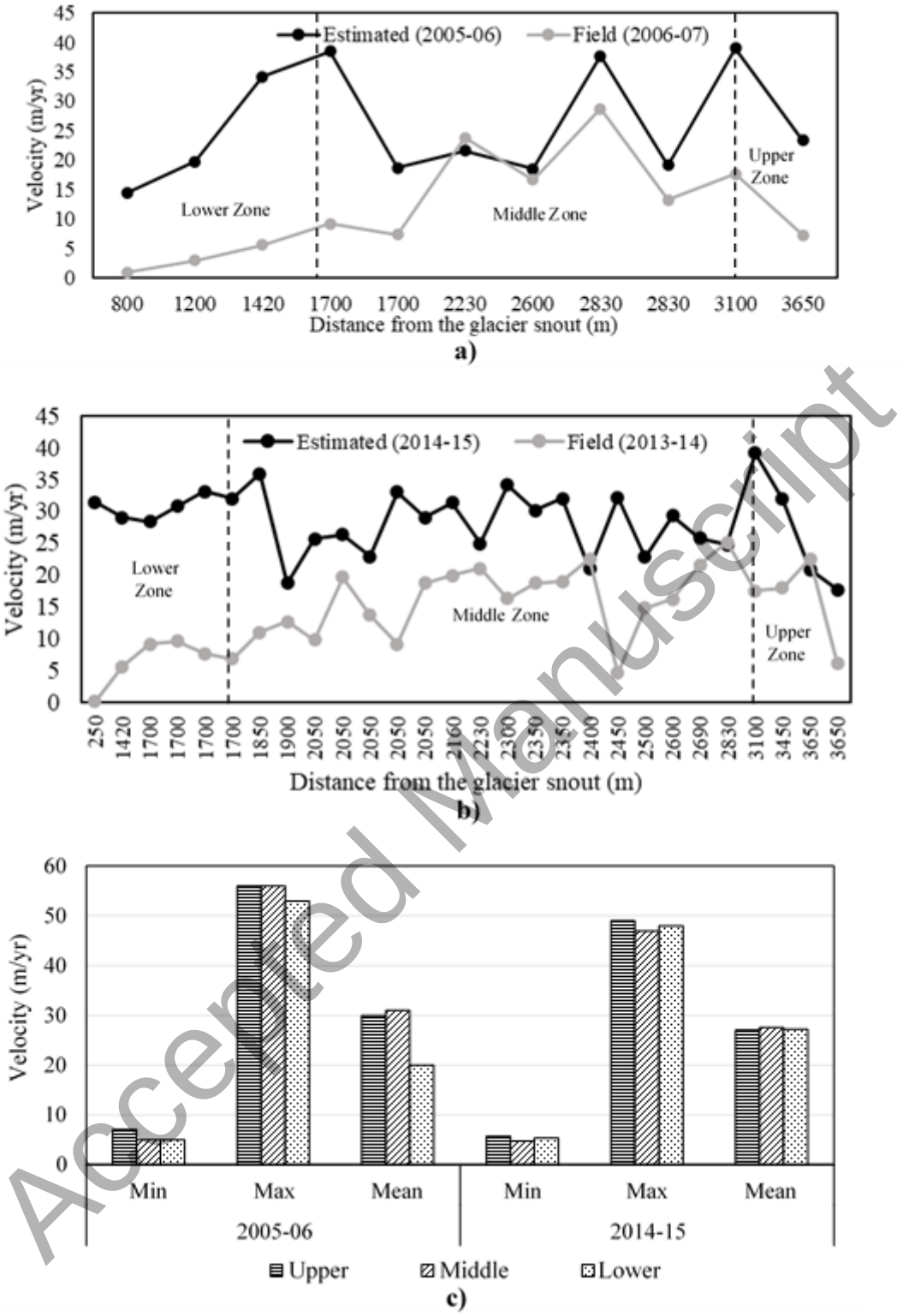

Figure 6. Estimated velocities along the central flowline of South Glacier for period a) 2005-06 and b) 2014-15. The field measurements close to the study period are also shown (Flowers et al., 2011; Farinotti et al., 2017). c) Zonal statistics of South Glacier estimates.

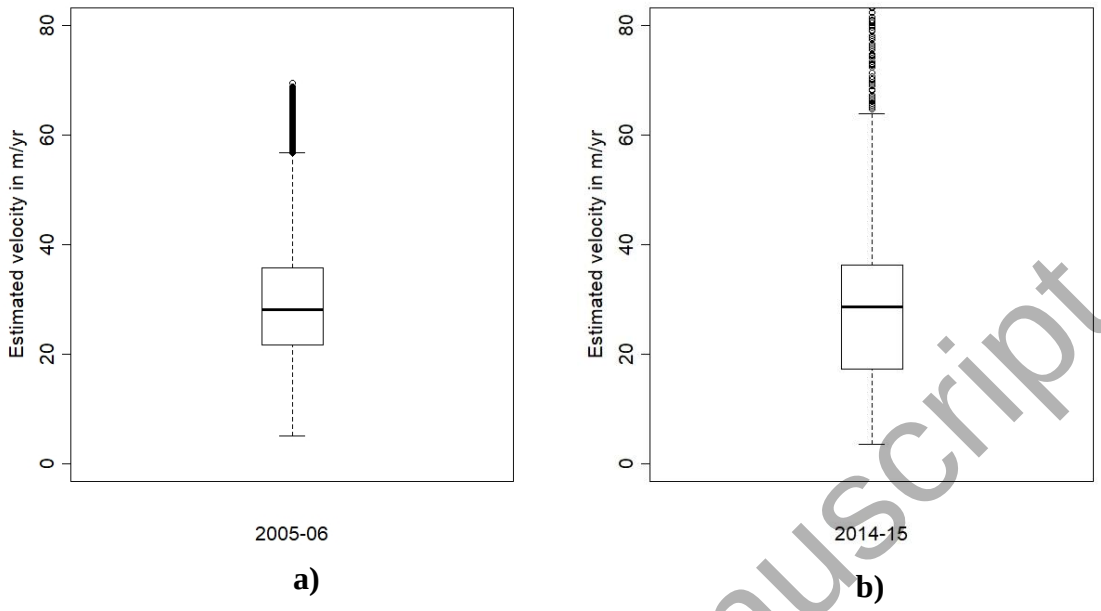

Figure 7. Boxplot of the surface velocity estimates of South Glacier for period a) 2005-06 and b) 2014-15.

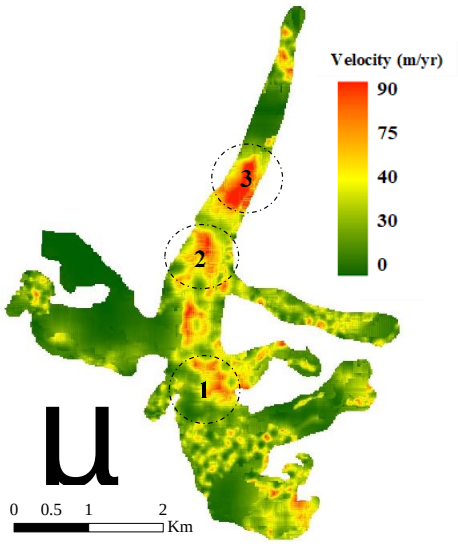

a)

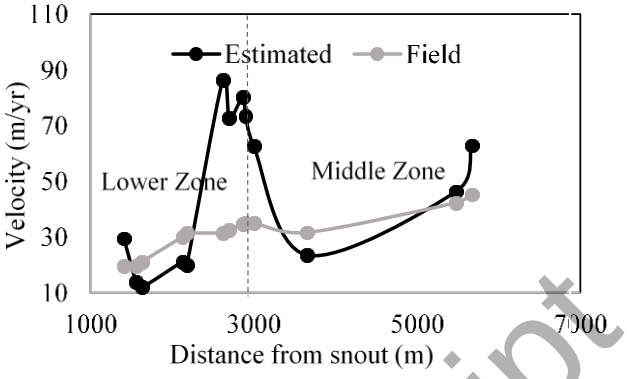

b)

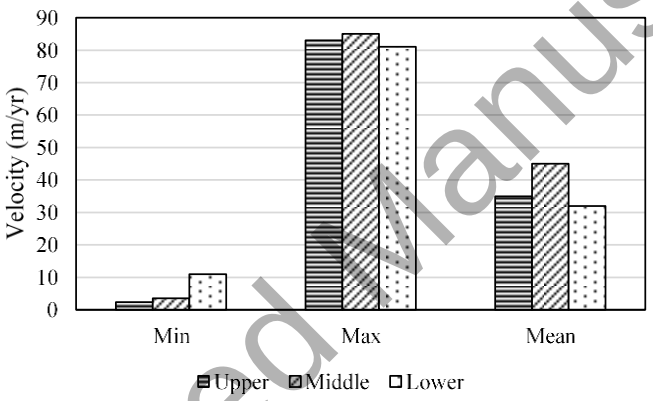

c)

Figure 8. a) Spatial distribution of the estimated surface velocity for period 2009-10 after smoothing. Circled areas of 1, 2 and 3 show the three zones with high velocity. b) Estimated and observed glacier annual surface velocity along the central flow line. c) Zonal statistics of Chhota Shigri Glacier velocity estimates for different zones.

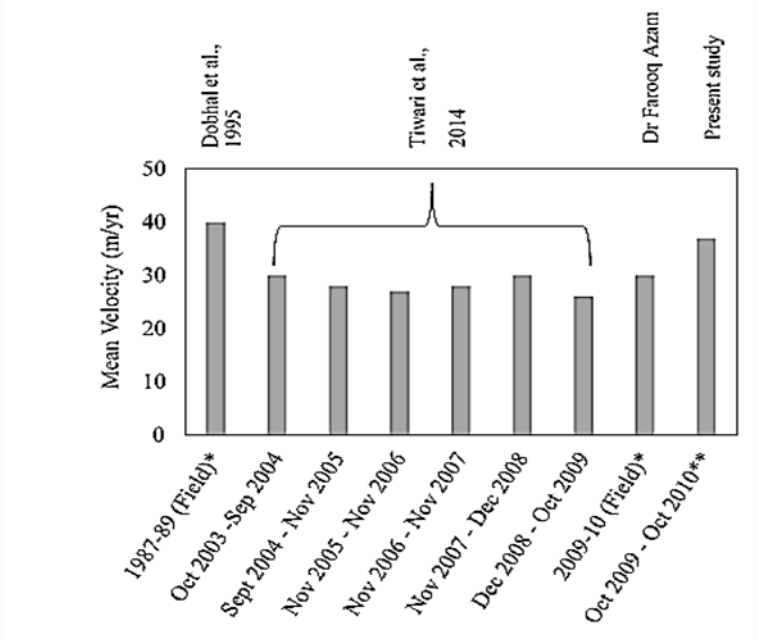

Figure 9. Glacier wide mean surface velocity trend of Chhota Shigri Glacier (field and estimated) for period 1987-2010. The glacier surface velocity estimates (period Oct 2003-Oct 2009) are taken from Tiwari et al. (2014). *Field measurements are taken from Dobhal et al., (1995) (period 1987-89) and Dr Farooq Azam (period 2009-10). **Estimated mean glacier surface velocity by the proposed method (Oct 2009 - Oct 2010).

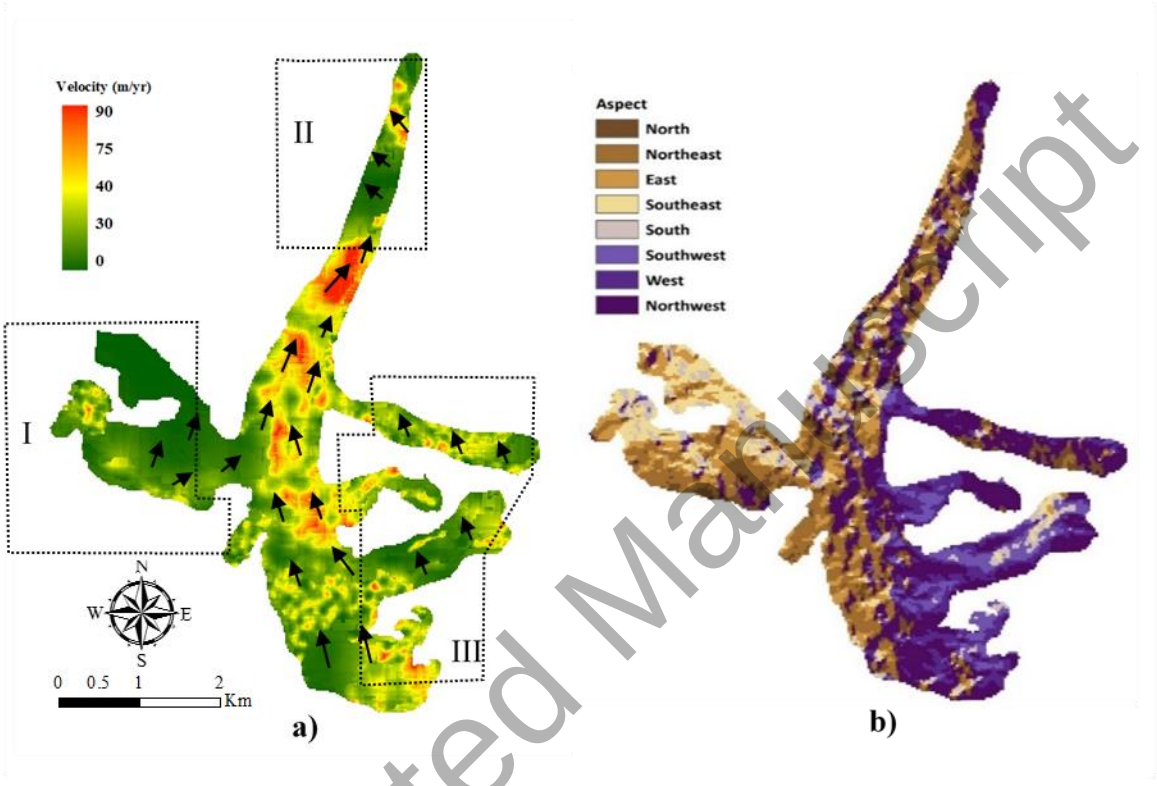

Figure 10. a) Direction of the estimated velocity of Chhota Shigri Glacier during the year 2009-10. The directions are shown by arrows. Regions I, II and II indicate the areas where the estimated flow direction mismatches the aspect map. b) Aspect map of the glacier.

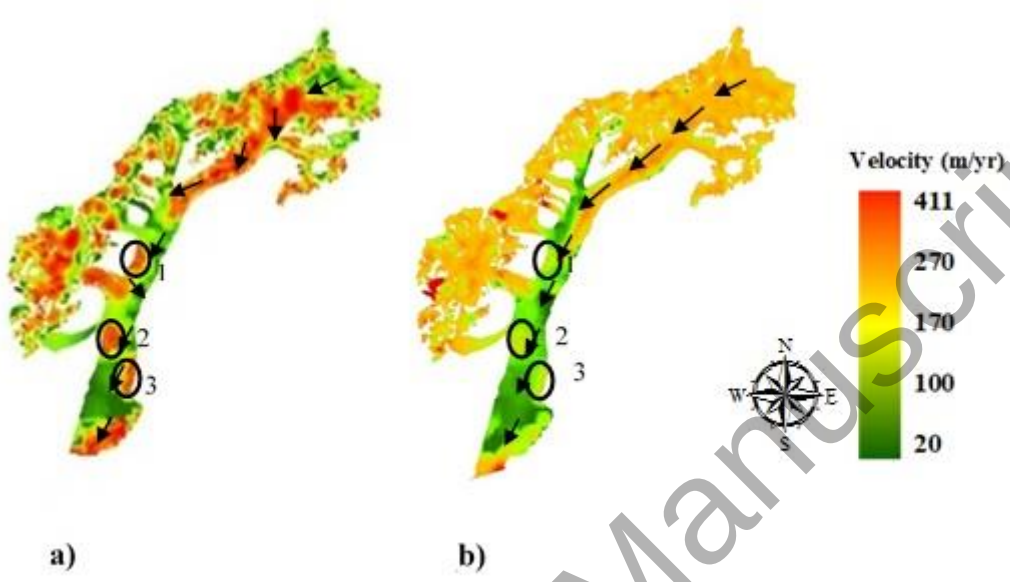

Figure 11. Spatial distribution of velocity estimates of Tasman Glacier for a) period 2005-06 using Envisat C-band VV polarized data and b) period 2007-08 using ALOS PALSAR L-band HH polarized data. Circled areas 1, 2 and 3 (in black) represent erroneous patches with unrealistic high surface velocity values.

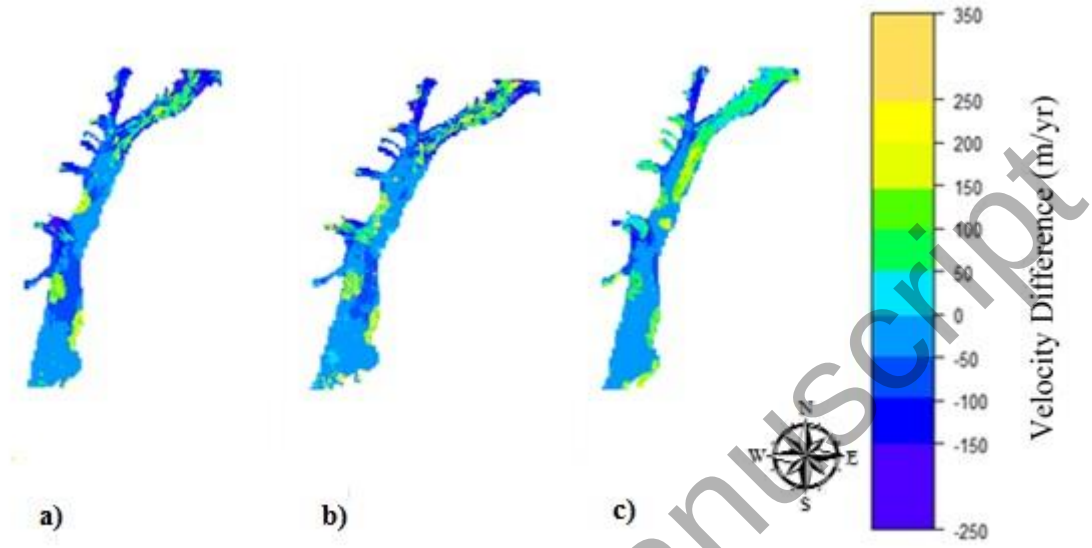

Figure 12. Difference between the velocity estimates and reference velocity (source: Farinotti et al., 2017), where the velocity estimates have been calculated for a) 2005-06 using Envisat (C-Band) without limiting the maximum window size, b) 2005-06 using Envisat (C-Band) after limiting the maximum window size. c) 2007-08 using ALOS PALSAR (L-Band) after limiting the maximum window size. Positive values show the overestimation and negative values show underestimation by the proposed approach.

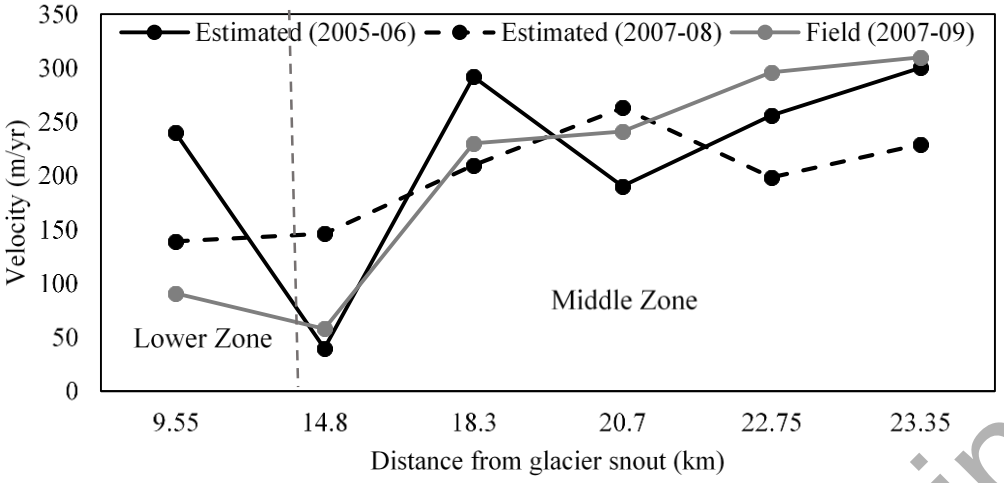

Figure 13. Estimated velocities of Tasman Glacier for period 2005-06 and 2007-08 compared with the field measurements close to the study period (source: Purdie et al., 2018).

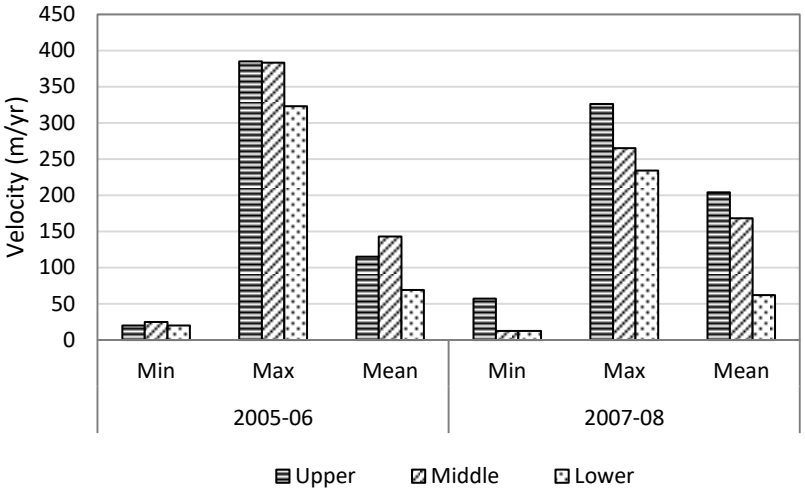

Figure 14. Zone-wise mean velocity estimates for the Tasman Glacier.

a)

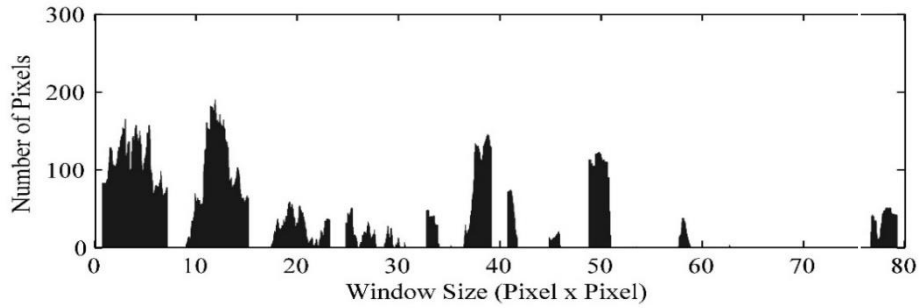

b)

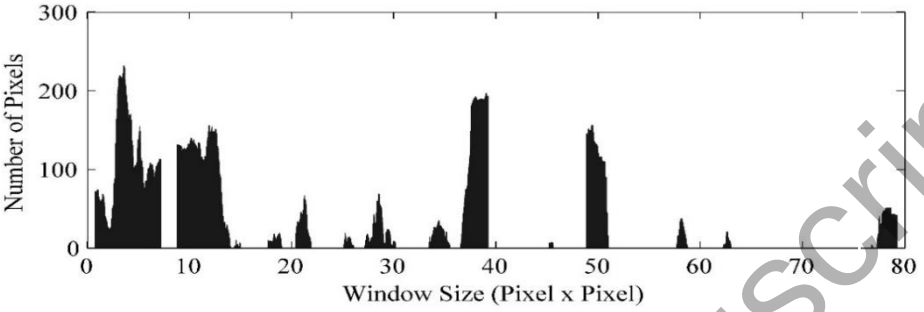

c)

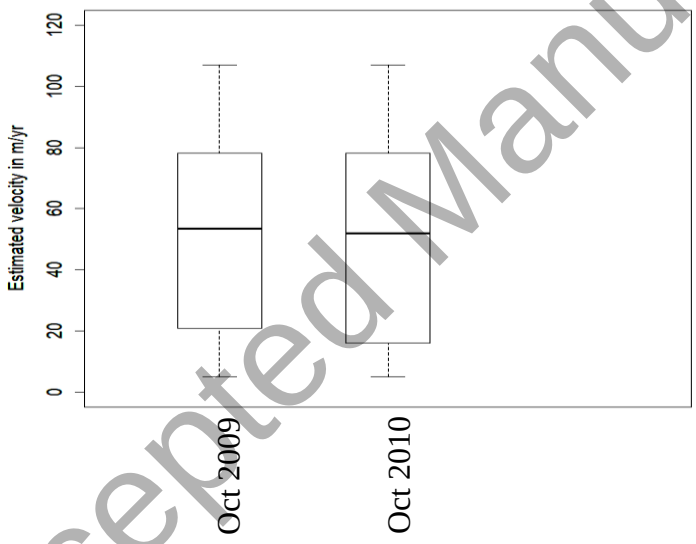

Figure 15. Window size distribution of Chhota Shigri Glacier using optical images of a) Oct, 2009 and b) Oct, 2010. c) The statistical distribution of surface velocity estimates using spatially varying window size obtained from a) & b).

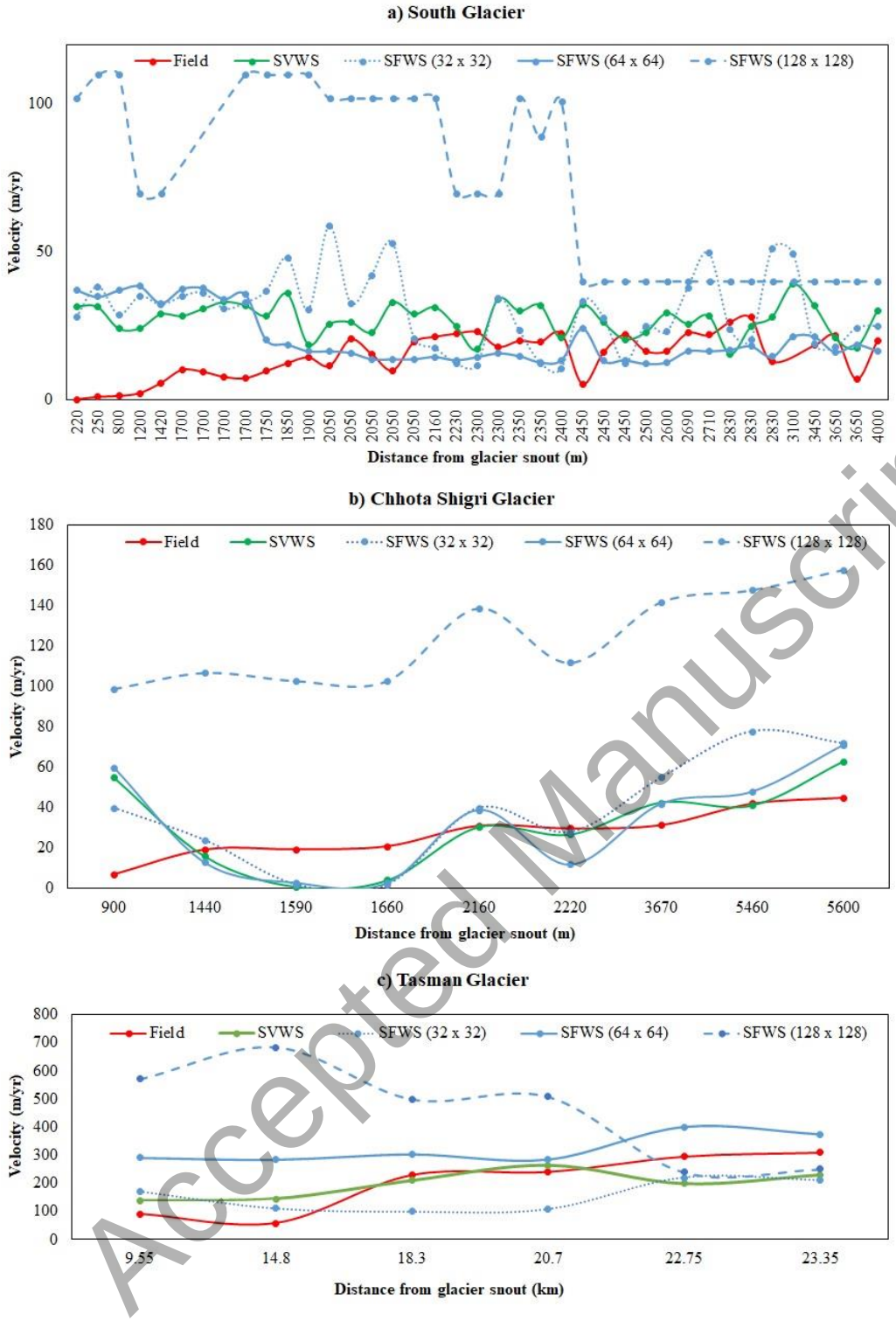

Figure 16. A comparative plot of the velocity estimates from the SWIFT method and the same maximum likelihood correlation but with spatially fixed window size (SFWS): a) South Glacier for period 2005-06, b) Chhota Shigri Glacier for period 2009-10, and c) Tasman Glacier for period 2007-08.

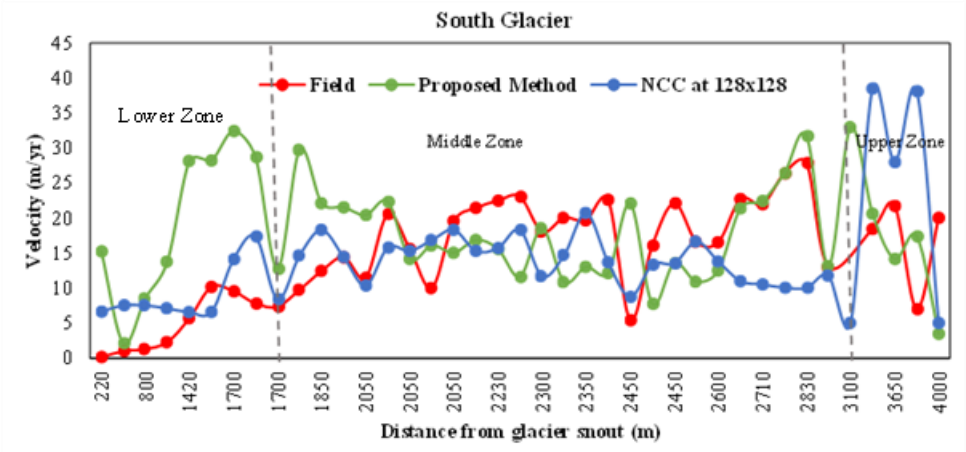

Figure 17. A comparative plot of proposed velocity estimates and cross correlation-based velocity estimates (at best performing window size) of: a) South Glacier for period 2005-06, b) Chhota Shigri Glacier for period 2009-10, and c) Tasman Glacier for period 2007-08.